Supporting information

Preparation and organic pollutants absorption behavior of new macroporous hydrophobic polyvinyl alcohol-formaldehyde sponges

Yanxiong Pan,[†,‡] Chao Peng,[†] Weicai Wang, [†,‡] Kai Shi,[†] Zhi Liu,[†] Xiangling Ji[†]*

[†] State Key Laboratory of Polymer Physics and Chemistry, Changchun Institute of Applied Chemistry, Chinese Academy of Sciences, Changchun 130022, P.R. of China

[‡] State Key Laboratory of Polymer Physics and Chemistry, Changchun Institute of Applied Chemistry, Chinese Academy of Sciences, University of the Chinese Academy of Sciences, Changchun 130022, P.R. of China.

E-mail: xlji@ciac.ac.cn

Tel & Fax: +86-0431-85262075

ATR-IR analysis

ATR-IR analysis was used to examine the characteristic chemical structure of PVF before and after hydrophobic modification. The IR spectra of pristine PVF, PVF-G_1, PVF-G_1-H_8, and PVF-G_1-H_{18} sponges are shown in Fig. S1-a. For pristine PVF sponge, the typical peaks at about 3200-3600 cm^{-1}, 2843-2943 cm^{-1}, 2778 cm^{-1}, and 1012 cm^{-1} are attributed to O-H stretching vibration, C-H stretching vibration of alkyl chain, C-H stretching vibration of aldehyde, and C-O-C vibration, respectively. The relative increases of the typical peaks of PVF-G_1 at 2843 -2943 cm^{-1} and 2778 cm^{-1} are related to the C-H stretching vibration of the alky chain and aldehyde, indicating the successful introduction of GA on the PVF sample. PVF-G_1-H_8, i.e., PVF-G_1 reacts with n-octanoyl chloride at 25 °C in acetonitrile, exhibits new peaks at 1734 cm^{-1} due to C=O stretching vibration. It also demonstrates increased intensity at 2922 cm^{-1} from methyl stretching vibration and at 2852 cm^{-1} from ethylene stretching vibration. The above results confirm the successful introduction of n-octanoyl group on PVF-G_1 sponges. For PVF-G_1-H_{18}, the appearance of new peaks at 1734 cm^{-1} from C=O stretching vibration and 721 cm^{-1} from rocking vibration of long-chain alkyl confirm the successful introduction of octadecyl chains on PVF-G_1. Compared with the low intensity of PVF-G_1-H_8 at 1734 cm^{-1}, 2922 cm^{-1}, and 2852 cm^{-1}, PVF-G_1-H_{18} exhibits relatively higher intensity along with low intensity at 3200 cm^{-1} to 3600 cm^{-1}, indicating the higher degree of substitution (DS) of PVF-G_1-H_{18}. PVF-G_1 reacts with the fatty acyl chloride with longer alkyl chain length, and shows higher DS (Fig. S1-b), which is probably attributed to the high reactivity of short-chain alkyl chloride tending to the side reaction, namely, the formation of carboxylic acid or ester. Under higher reaction temperature, more alkyl chains can be anchored onto the network of samples (Fig. S1-c), whereas the feed ratio

of [GA]/[OH] and pristine apparent density have almost no influence on the further substitution of hydroxyl group with fatty acyl chloride (Figs. S1-d and S1-e, respectively).

Solid-state CP/MAS ^{13}C NMR analysis

Solid-state CP/MAS ^{13}C NMR spectroscopy was used to characterize the structures of as-prepared PVF sponges. Typical spectra of PVF, PVF-G_1, PVF-G_1-H_8, and PVF-G_1-H_{18} are shown in Fig. S2-a. PVF and PVF-G_1 possess similar chemical shifts, and the region from 84.6 ppm to 101.7 ppm is attributed to methylene C_a of the six-membered cyclic acetal. The signal peak at about 58.5 ppm to 83.8 ppm is a representative peak for methines C_b, C_c, and C_e. The new peaks at 15.1 ppm and 172.7 ppm of both PVF-G_1-H_8 and PVF-G_1-H_{18} represent methyl C_g and carboxyl C_f in the obtained networks, indicating the successful substitution of hydroxyl group with hydrophobic alky chains. The DS calculated from the integration of the corresponding resonance[1-3] is listed in Table 1. For example, the DS of PVF-G_1-H_m, substituted with different alkyl chain lengths, i.e. C_4, C_8, C_{12}, C_{16}, and C_{18} (Fig. S2-b) are 32.3%, 45.6%, 43.3%, 44.8%, and 54.1%, respectively. This increased trend is similar to the ATR-IR results. The DSs of PVF-G_1-H_{18} prepared at 25, 50, and 75 °C are 54.1%, 55.0%, and 62.3% (Fig. S2-c), respectively. These findings indicate that samples with slightly higher DS could be obtained by increasing the acylation reaction temperature. The DSs of PVF-G_0-H_{18}, PVF-G_1-H_{18}, PVF-G_2-H_{18}, and PVF-G_4-H_{18} are 50.1%, 54.1%, 45.3%, and 50.0% (Fig. 2-d), respectively. The DSs of PVF-G_1-H_{18}–0.059, PVF-G_1-H_{18}–0.073, PVF-G_1-H_{18}–0.095, and PVF-G_1-H_{18}–0.110 are approximately 55.3%, 54.1%, 57.8%, and 60.8% (Fig. S2-e), respectively, indicating that the feed ratio of [GA]/[OH] and the apparent

density of pristine PVF have no obvious influence on the DS of hydroxyl group with long alkyl chain, which is probably attributed to acetalization reaction characteristics and open-cell structure of the samples.

Apparent density

Apparent densities of PVF sponges are listed in Table 1. Pristine PVF sponge has an apparent density of 0.073 $g \cdot cm^{-3}$. A series of PVF-$G_{1\text{-}4}$ sponges, i.e., further crosslinking using GA with pristine PVF, has almost the similar apparent density as that of the pristine sample, ranging from 0.069 $g \cdot cm^{-3}$ to 0.072 $g \cdot cm^{-3}$ in the reasonable error. After introducing alkyl chains, such as C_4-C_{18}, onto the PVF framework, the apparent densities exhibit a slight fluctuation in the range of 0.071-0.079 $g \cdot cm^{-3}$. However, it implies that hydrophobic PVF sponges have similar apparent densities as the initial sample. The above results indicate that GA crosslinking and alkyl chain substitution have no substantial influence on apparent density of PVF sponges, which is probably attributed to the simultaneous slight increase in both volume and mass after substitution of hydrophobic alkyl chains (Table 1).

Porosity, Pore size and distribution ,

A mercury intrusion porosimeter was used to characterize pore size and distribution of different samples. The typical pore size distribution curves of as-prepared PVF, PVF-G_1, PVF-G_1-H_8, and PVF-G_1-H_{18} are shown in Fig. S3-a. All four samples exhibit monomodal pore size distribution, with a dominant pore size at about 60 μm. The porosities of the above four samples are 95.0%, 97.3%, 95.2%, and 89.7%, respectively, demonstrating that the PVF before and after hydrophobic modification still possesses high porosity. The porosities of PVF-G_0-H_{18}, PVF-G_1-H_{18}, PVF-G_2-H_{18}, and PVF-G_4-H_{18} are 88.1%, 89.7%, 92.3%, and 93.5%, respectively, indicating that more GA leads

to high porosity (Fig. S3-b). Such result may be attributed to the introduction of GA in improving the mechanical properties of obtained PVF-G_n-H_{18} sponges effectively, which facilitates the intrusion of mercury into the pores during tests and weakens the deformation of pore structures.[4]

In addition, the porosities of PVF-G_1-H_4, PVF-G_1-H_8, PVF-G_1-H_{12}, PVF-G_1-H_{16}, and PVF-G_1-H_{18} are 93.6%, 95.2%, 90.1%, 92.7%, and 89.7%, respectively (Fig. S3-c). And the porosities of PVF-G_1-H_{18} prepared at 50 °C and 75 °C are 92.8% and 92.5% (Fig. S3-d), respectively. The porosities of PVF-G_1-H_{18}-0.059, PVF-G_1-H_{18}-0.073, PVF-G_1-H_{18}-0.095, and PVF-G_1-H_{18}-0.110 are 90.7%, 89.7%, 91.4%, and 90.4%, respectively, indicating that pristine apparent density of sponges has almost no influence on final porosity. As shown in Fig. S3-e, all samples exhibit a unimodal macropore size distribution with a peak centered at about 60 μm except PVF-G_1-C_{18}-0.059 (at about 90.7 μm). The above results indicates that the original pore structure and pore channels of pristine PVF are well maintained after the hydrophobic modification of sponges.

1. Pollers, I.; Adriaensens, P.; Carleer, R.; Vanderzande, D.; Gelan, J., 1H and 13C NMR spectroscopy as a tool to probe the microstructures of different types of poly(vinyl formal). *Macromolecules* **1996,** *29* (18), 5875-5881.

2. Adriaensens, P.; Pollers, I.; Carleer, R.; Vanderzande, D.; Gelan, J., Solid-State NMR study of different types of poly(vinyl formal). *Macromolecules* **1998,** *32* (2), 440-447.

3. Wang, Y.; Ono, H.; Ikeda, A.; Hori, N.; Takemura, A.; Yamada, T.; Tsukatani, T., 1H NMR and 13C NMR investigations of sequence distribution and tacticity in poly(vinyl alcohol-co-vinyl levulinate)**.** *Polymer* **2006**, *47* (22), 7827-7834.

4. Washburn, E. W., The dynamics of capillary flow. *Physical Review* **1921,** *17* (3), 273-283.

List of Figures

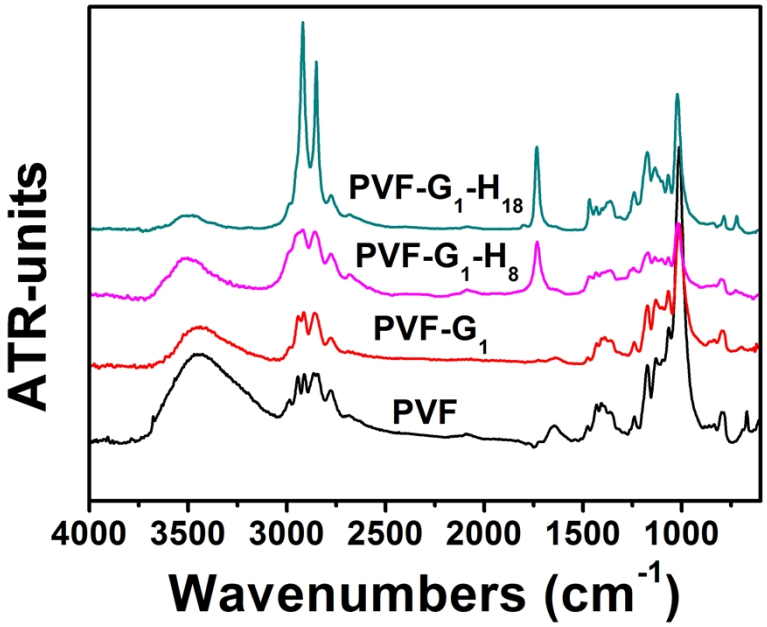

Figure S1-a. FTIR spectra of pristine PVF, PVF-G_1, PVF-G_1-H_8 and PVF-G_1-H_{18}.

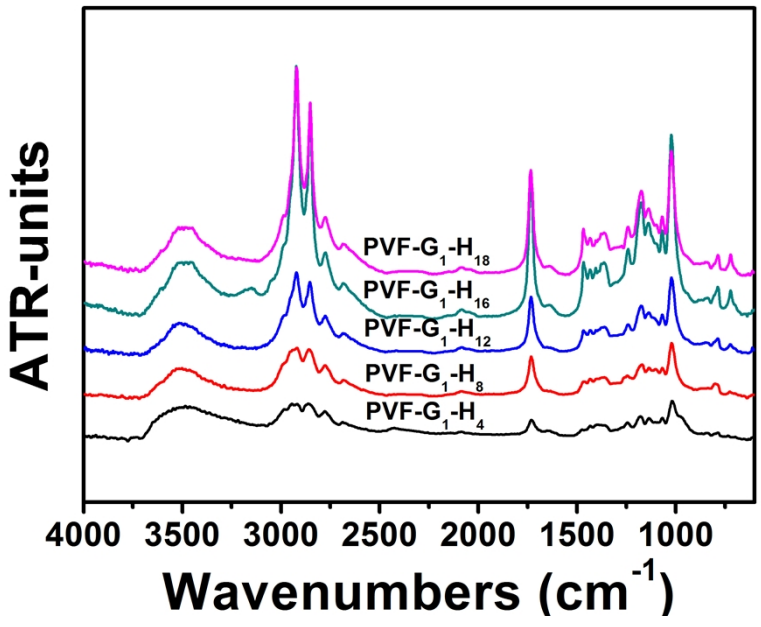

Figure S1-b. FTIR spectra of PVF-G_1-H_ms with various alkyl chain length.

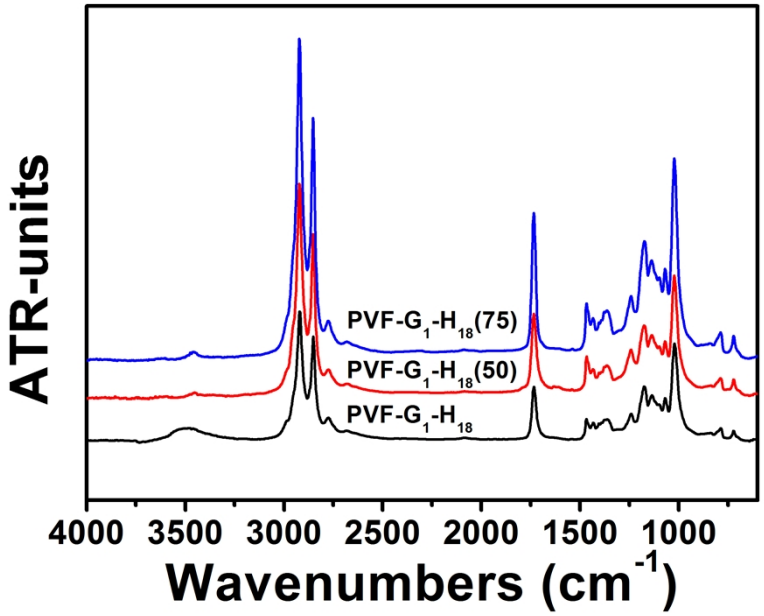

Figure S1-c. FTIR spectra of PVF-G_1-H_{18}s prepared at different temperature.

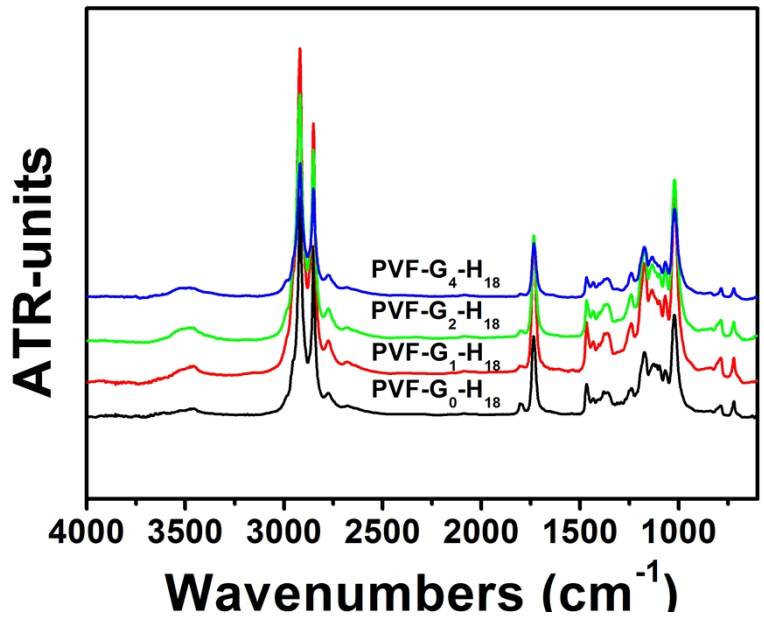

Figure S1-d. FTIR spectra of PVF-G_n-H_{18}-Hs with different feed ratio of [GA]/[OH].

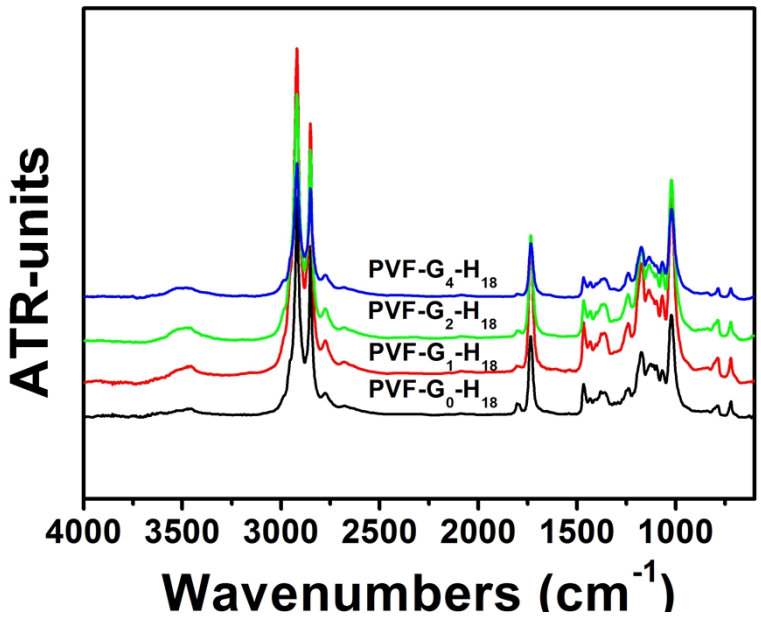

Figure S1-e. FTIR spectra of PVF-G_1-H_{18}s with various apparent density.

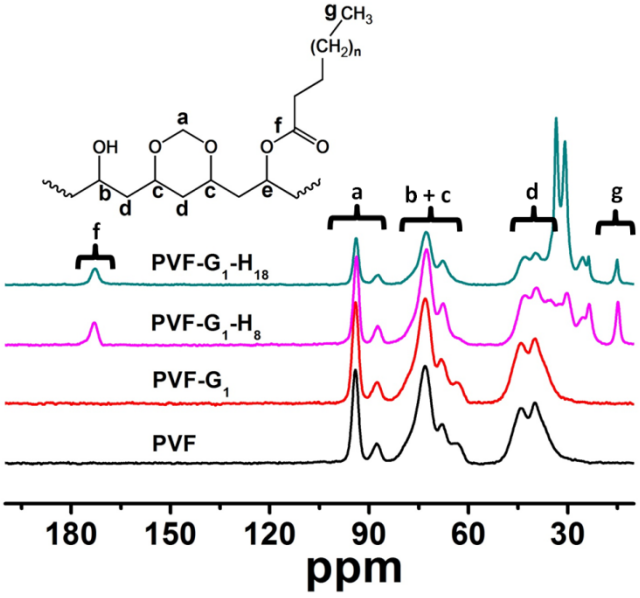

Figure 2-a. Solid-state CP/MAS ^{13}C NMR spectra of pristine PVF, PVF-G_1, PVF-G_1-H_8 and PVF-G_1-H_{18} at 25 ^oC.

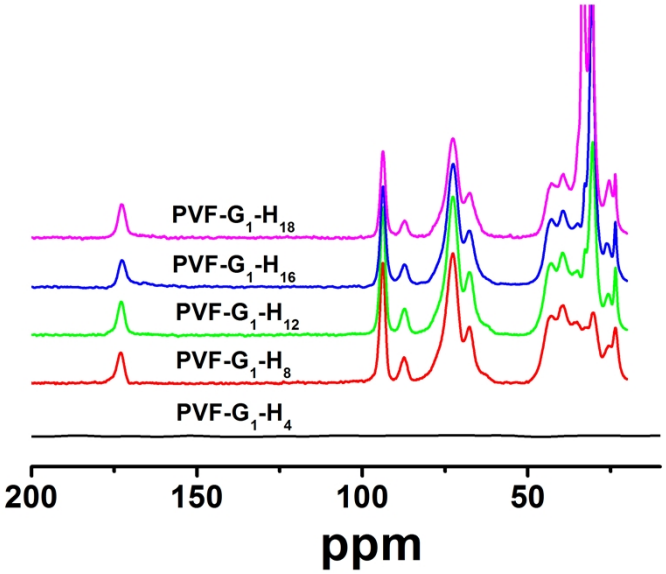

Figure S2-b. Solid-state CP/MAS ^{13}C NMR spectra of PVF-G_1-H_ms with various alkyl chain length.

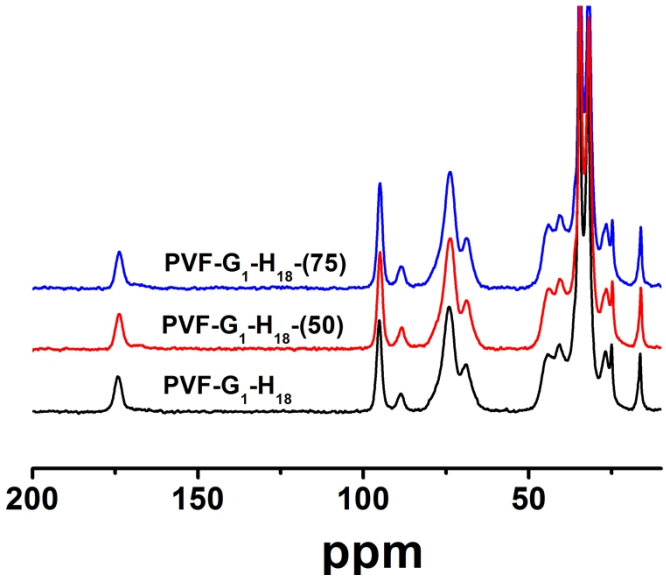

Figure S2-c. Solid-state CP/MAS ^{13}C NMR spectra of PVF-G_1-H_{18}s prepared at different temperature.

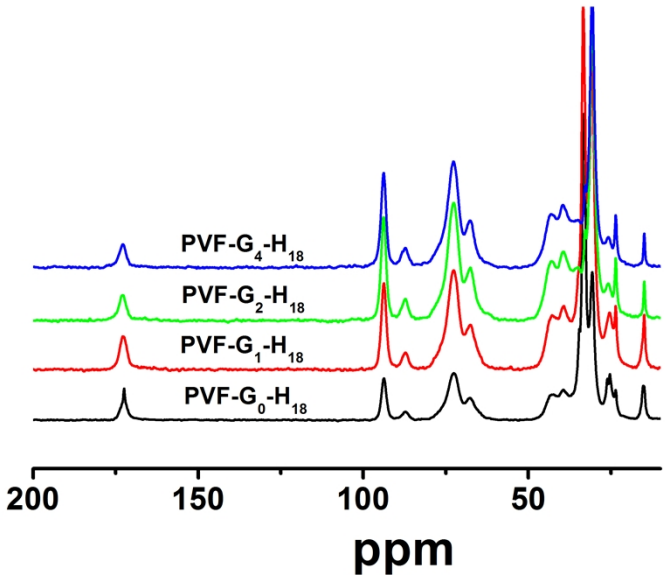

Figure S2-d. Solid-state CP/MAS ^{13}C NMR spectra of PVF-G_n-H_{18}s with different feed ratio of [GA]/[OH].

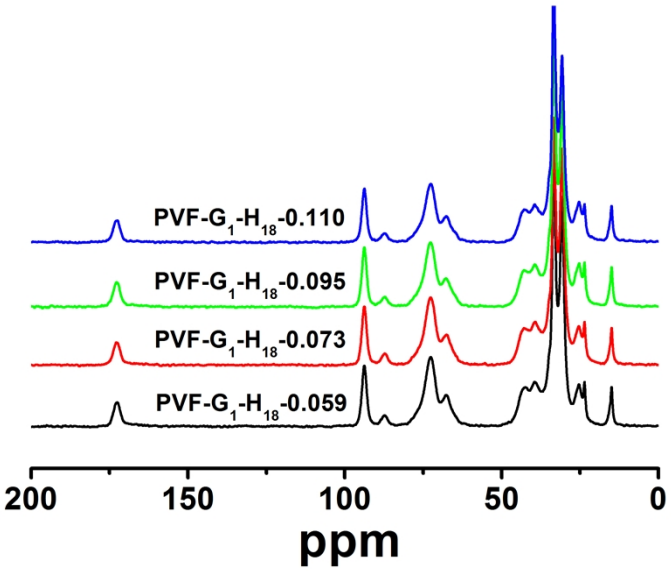

Figure S2-e. Solid-state CP/MAS ^{13}C NMR spectra of PVF-G_1-H_{18}s with different pristine apparent density.

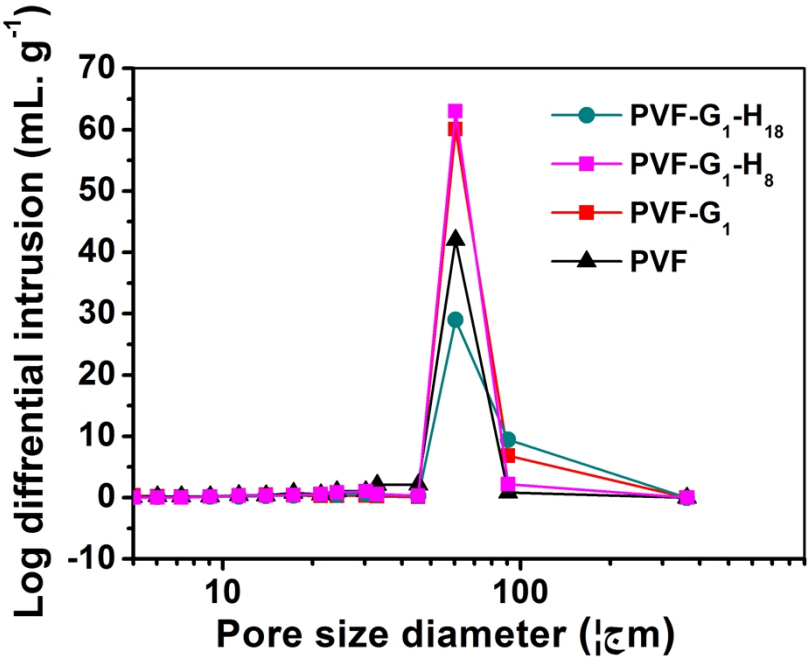

Figure S3-a. Pore size distributions of pristine PVF, PVF-G_1, PVF-G_1-H_8 and PVF-G_1-H_{18}.

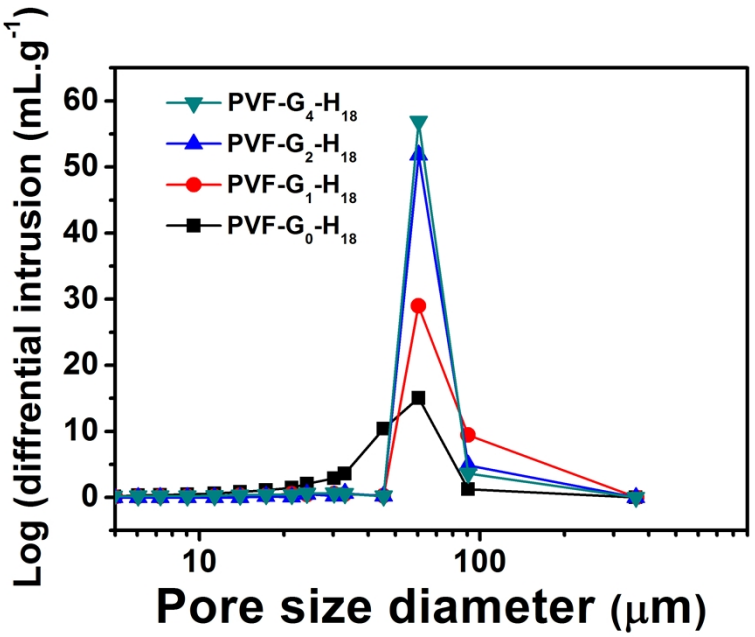

Figure S3-b. Pore size distributions of PVF-Hs with different GA feed amount.

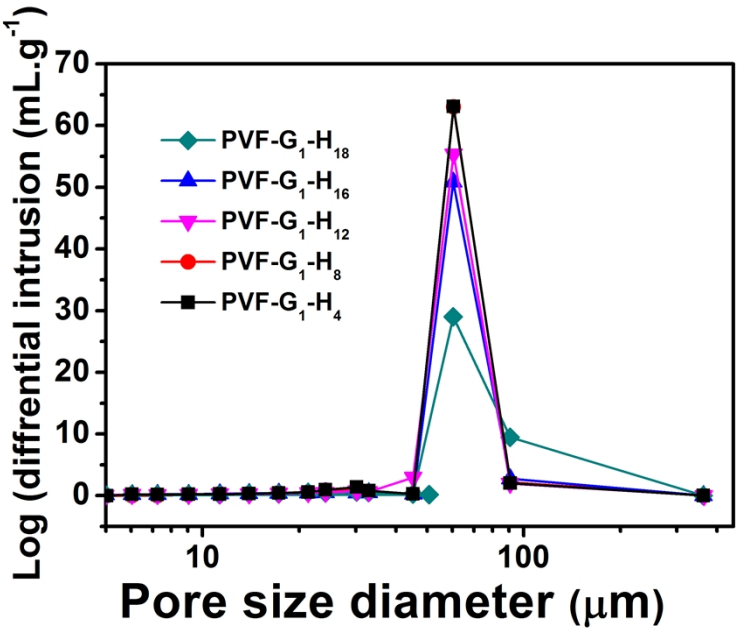

Figure S3-c. Pore size distributions of PVF-Hs with different alkyl chain length.

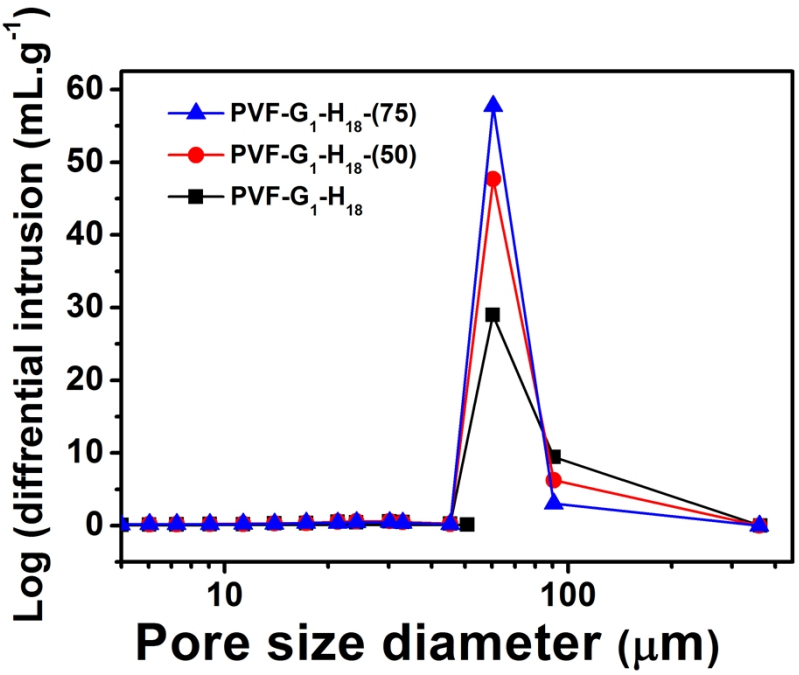

Figure S3-d. Pore size distributions of PVF-Hs prepared at different temperature.

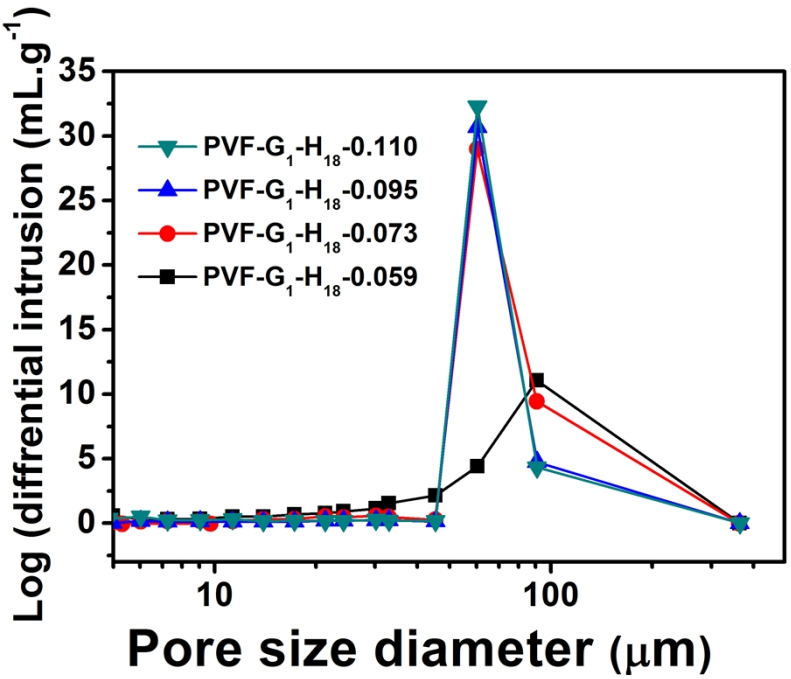

Figure S3-e. Pore size distributions of PVF-Hs with different apparent density.

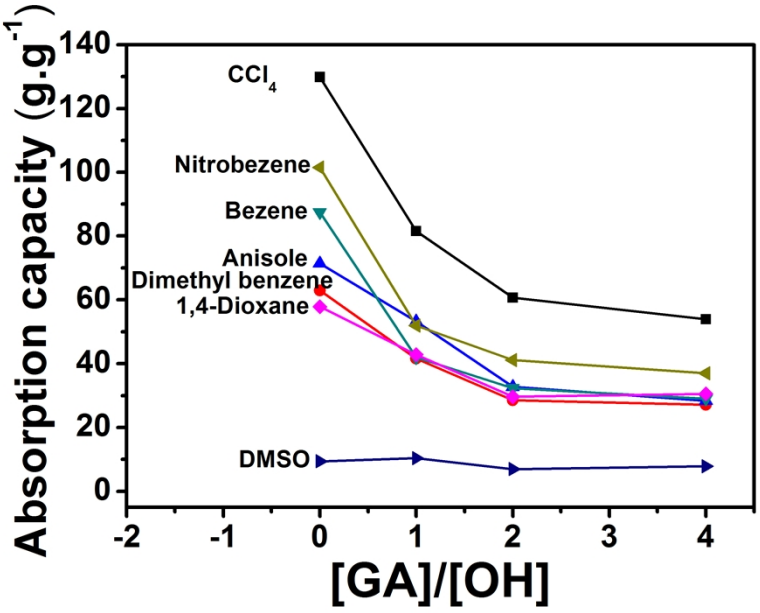

Figure S4. The effect of GA feed ratio on the absorption capacity of PVF-$G_{0\text{-}4}$-H_{18}s for various organic solvents.

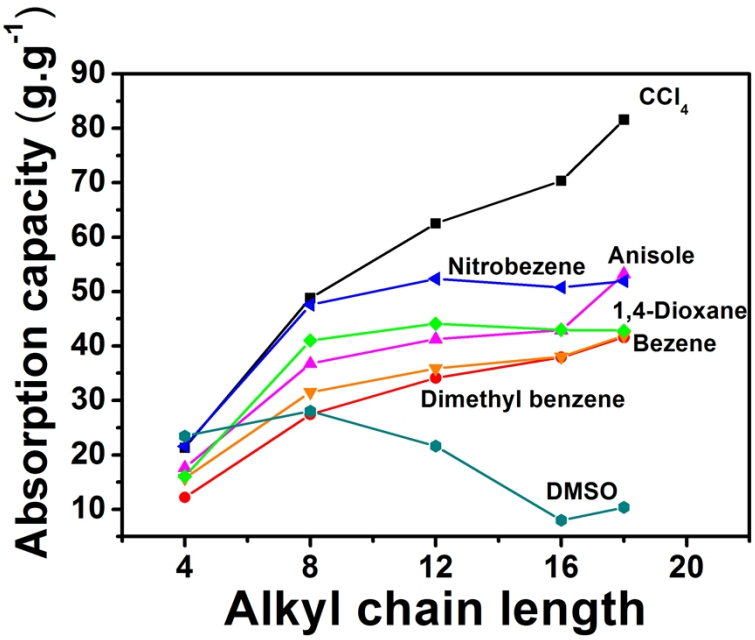

Figure S5. The effect of alkyl chain length on the absorption capacity of PVF-G_1-$H_{4\text{-}18}$s for various organic solvents.

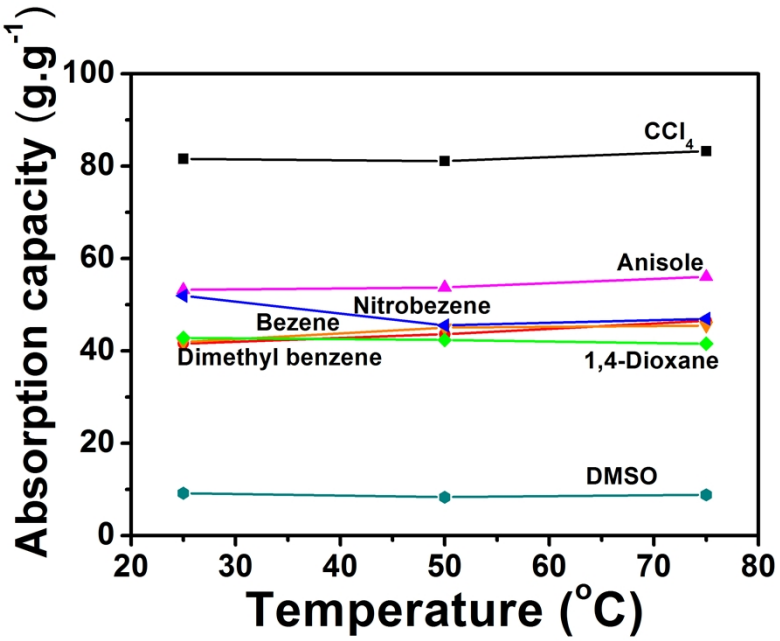

Figure S6. The effect of reaction temperature on the absorption capacity of PVF-G_1-$H_{4\text{-}18}$s for various organic solvents.

Table S1. The physical constants of tested organic solvents

	Dielectric constant	Solubility parameters ($cal^{1/2}.cm^{-3/2}$)	Density ($g.cm^{-3}$)
n-Hexane	1.90	7.24	0.66
1,4-Dioxane	2.21	10.00	1.04
Carbon tetrachloride	2.23	8.65	1.60
Benzene	2.27	9.15	0.88
Dimethyl benzene	2.38	8.75	0.86
Toluene	2.38	8.91	0.87
Anisole	4.30	9.13	1.48
Chloroform	4.81	9.21	1.48
Chlorobenzene	5.61	9.57	1.10
THF	7.58	9.52	0.89
Dichloromethane	8.90	9.73	1.33
Nitrobenzene	34.60	10.62	1.21
DMF	36.71	12.14	0.94
DMSO	48.90	13.40	1.10